Tunable Raman photons in singly charged p-doped quantum dots

F. Carreño and M.A. Antón

Facultad de Óptica y Optometría, Universidad Complutense de Madrid,

C/ Arcos de Jalón 118, 28037 Madrid, Spain

(Dated: February 16, 2016)

Abstract

The obtention of spontaneous Raman photons is analyzed in singly charged p-doped quantum dots in the absence of an external magnetic field. The use of a far detuned single driving laser allows to obtain a Raman photon line which exhibits subnatural linewidth, and whose center can be tuned by changing the detuning and/or the Rabi frequency of the driving field. The Raman photons are produced along the undriven transition and they arise from the weak interaction of the trion states with the nuclear spins. The operating point for the gate voltage of the heterostructure can also be used to modify the linewidth and the peak value of the fluorescent signal.

I. INTRODUCTION

Optical properties of Quantum Dots (QDs) closely resemble those found in real atoms. They have been proposed as a basic unit to implementing qubits due to their large coherence times and their relatively high immunity to the surrounding environment[1]. Coherent manipulation of exciton wave-functions[2], optical pumping[3–9], partial rotations of the spin vector[10–13], resonance fluorescence[14–20], and single photon generation[22–24] are some of the challenging experiments which have revealed their potential in the field of quantum information science.

Quantum entanglement plays a central role in quantum repeaters. The underlying protocol requires the creation of entanglement between two distant emitters by making the single photons arising from them to spectrally overlap on a beam splitter[25]. Such entanglement previously demonstrated in ions[26], atoms[27], NV centers[28], has been recently demonstrated in p-doped QDs in the Voigt geometry[29]. In the latter system, the entanglement generation relies on the application of far detuned pulses which produce Raman photons[30], whose detection projects the composite system wave-function onto the desired entangled state.

The aim of this work is to extend previous investigations on the production of Raman photons carried out in n-doped QDs in the Voigt geometry[30]. Here we consider p-doped QDs in the absence of an external magnetic field. The paper is organized as follows: Section II establishes the model, i.e., the Hamiltonian of the system and the keys of the main dissipative processes which are needed to derive the time-evolution equations of the atomic operators. We also presents the basis for the analysis of the spectral properties of the fluorescent photons when the system is driven by a far detuned coupling laser. Section III presents numerical results assuming typical data for QD taken from experimental studies. Finally, Section IV summarizes the main conclusions.

II. THEORETICAL MODEL

We consider InAs/GaAs Stranski-Krastanov self-assembled QDs with growth direction along the Z-axis. The QDs are separated from a Fermi sea of holes by several nanometers in thick p-doped back contact layer. An external bias voltage applied between the top gate and the back contact allows the charge of the QD. The ground hole states are labeled $|1\rangle \equiv |\Downarrow\rangle$

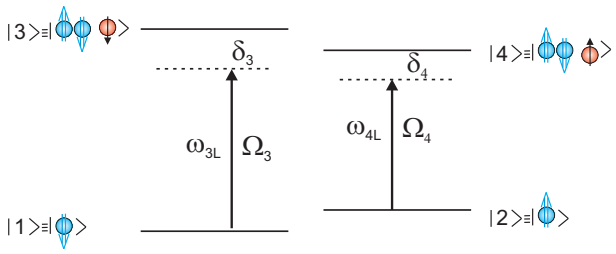

FIG. 1. Four level scheme illustrating the ground and excited states of self-assembled QDs. In the absence of an external magnetic field both the ground and excited states are degenerate. Transition $|1\rangle \leftrightarrow |3\rangle (|2\rangle \leftrightarrow |4\rangle)$ is driven by a $\sigma^+(\sigma^-)$ laser field with Rabi frequency $\Omega_3(\Omega_4)$ and optical detuning $\delta_3(\delta_4)$.

and $|2\rangle \equiv |\Uparrow\rangle$, while the excited trion states are $|4\rangle \equiv |\Downarrow \Uparrow \uparrow\rangle$ and $|3\rangle \equiv |\Downarrow \Uparrow \downarrow\rangle$. Here $\Uparrow$ ($\Downarrow$) and $\uparrow$ ($\downarrow$) denote a heavy hole (HH) and an electron with spins along (against) the Z-axis. The energy level diagram is depicted in Fig. 1. The optical transition $|1\rangle \leftrightarrow |3\rangle (|2\rangle \leftrightarrow |4\rangle)$ is driven by a $\sigma^+(\sigma^-)$ polarized laser field, while transitions $|1\rangle \leftrightarrow |4\rangle$ and $|2\rangle \leftrightarrow |3\rangle$ remain dark due to selection rules. The application of an external magnetic field along the Z-axis, in the so-called Faraday geometry, lifts the degeneracy of hole/electron levels according to $E_{Zm}^{h(e)} = \frac{1}{2}\mu_B g^{h(e)} B_z$, where $E_{Zm}^{h(e)}$ stands for the Zeeman energy shift relative to $B_z = 0$ T, B_z and μ_B being the external magnetic field and the Bohr magneton, respectively. Quantity $g^{h(e)}$ is the Landé factor of carrier $h(e)$.

The Hamiltonian that governs the dynamics of the QD can be expressed as

$$H = H_A + H_{Int} + H_{ns} \ . \tag{1}$$

The free Hamiltonian H_A of the four-level QD system reads

$$H_A = \sum_{j=1}^{4} E_j \sigma_{jj} \ , \tag{2}$$

where $E_j = \hbar\omega_j$ is the energy of the j-th QD level and σ_{ij} are the Pauli operators of the excitation electron-hole pair.

The interaction Hamiltonian H_{Int} is taken in the rotating-wave approximation

$$H_{Int} = \hbar\Omega_3 e^{i\omega_{3L}t}\sigma_{13} + \hbar\Omega_4 e^{i\omega_{4L}t}\sigma_{24} + H.c. \ , \tag{3}$$

and it accounts for the interaction of the QD with the optical fields of angular frequencies ω_{3L}, and ω_{4L} which drive transitions $|1\rangle \leftrightarrow |3\rangle$, and $|2\rangle \leftrightarrow |4\rangle$, respectively. The Rabi

frequencies are explicitly given by $\Omega_3 = \vec{\mu}_{13} \cdot \vec{E}_3/2\hbar$, and $\Omega_4 = \vec{\mu}_{24} \cdot \vec{E}_4/2\hbar$, $\vec{E}_3$ and $\vec{E}_4$ being the slowly varying amplitudes of the optical fields. Finally, H_{ns} is the part of the Hamiltonian which accounts for the electron spin interaction with the nuclear spins which can be modeled as

$$H_{ns} = \hbar\Omega_N \sigma_{34} + H.c. \,, \tag{4}$$

where $\Omega_N = g_e \mu_B B_{int}^{xy}/\hbar$ is the angular Rabi frequency of the exciton electron spin precession, and B_{int}^{xy} stands for the in-plane internal magnetic Overhauser field. In arriving at Eq. (4) we have considered the interaction of a localized electron spin with the surrounding nuclear spin ensemble given by[31]: $H_{hyp}^{e} = \frac{\nu_0}{8} \sum_i A_i^e \left|\psi(R_i)\right|^2 (\hat{\mathbf{I}}_\mathbf{i} \cdot \hat{\sigma})$, where ν_0 is the volume of the unit cell, $\psi(R_i)$ is the electron envelope wave function at the i-th nucleus, $\hat{\mathbf{I}}_\mathbf{i}(\hat{\sigma})$ stands for the spin operator of $i-th$ nuclear(electron) spin and the sum runs over all nuclei i in the lattice. A_i^e is the hyperfine coupling strength determined by the value of the electron wave function at the site of each nucleus. We resort to describing the effect of hyperfine interaction through an effective magnetic field felt by the QD spin, the so-called Overhauser field: $\mathbf{B_N} = \frac{\nu_0}{8} \frac{A^e}{g_e \mu_B} \langle \sum_i \hat{\mathbf{I}}_\mathbf{i} \rangle$, where A^e is an average spin-nuclei coupling constant. Due to the arbitrary direction of the Overhauser field, the spin excited states become admixed. For the kind of situations considered in this work, we can treat the hyperfine field as a purely classical field with correlation time in the millisecond scale. Thus assuming that the nuclear field is described through a Gaussian distribution of zero mean and with variance B_{nuc}, the hyperfine interaction reduces to the one given in Eq. (4). Note that the z component of $\mathbf{B_N}$ only leads to a small Zeeman splitting which is reabsorbed into the energy of the upper levels. A similar approach was used by Dreiser et al. 32 to describe the effect of hyperfine interaction through an effective magnetic field. Typical values of B_{nuc} range from $9 - 30$ mT[9,32]. The hyperfine interaction of the hole with the spin nuclei H_{hyp}^{h} can be considered to be negligible to leading order due to the p-like symmetry of the hole Bloch wave function. Measurements on individual QDs using optical detection with a high spectral resolution allow for measuring simultaneously the hole Overhauser shift and that for the electron: the ratio between the all-element-averaged hole A^h and electron (A^e) was found to be $A^h/A^e \approx -0.1$ in InP and InGaAs QDs[33].

The dissipative processes are described through operator $\mathcal{L}\rho$ which in the Linblad form

reads as

$$\begin{aligned}\mathcal{L}\rho = &\Gamma_{12}\sigma_{21}\rho\sigma_{12} - \frac{\Gamma_{12}}{2}\left(\sigma_{11}\rho + \rho\sigma_{11}\right)\\ &+\Gamma_{21}\sigma_{12}\rho\sigma_{21} - \frac{\Gamma_{21}}{2}\left(\sigma_{22}\rho + \rho\sigma_{22}\right)\\ &+\Gamma_{34}\sigma_{43}\rho\sigma_{34} - \frac{\Gamma_{34}}{2}\left(\sigma_{33}\rho + \rho\sigma_{33}\right)\\ &+\Gamma_{43}\sigma_{34}\rho\sigma_{43} - \frac{\Gamma_{43}}{2}\left(\sigma_{44}\rho + \rho\sigma_{44}\right)\\ &+\Gamma_{0}\sigma_{24}\rho\sigma_{42} - \frac{\Gamma_{0}}{2}\left(\sigma_{44}\rho + \rho\sigma_{44}\right)\\ &+\Gamma_{0}\sigma_{13}\rho\sigma_{31} - \frac{\Gamma_{0}}{2}\left(\sigma_{33}\rho + \rho\sigma_{33}\right)\ . \end{aligned} \tag{5}$$

The terms involving Γ_0 arise from Linblad operators $L_1(\sqrt{\Gamma_0}\sigma_{13})$, and $L_2(\sqrt{\Gamma_0}\sigma_{24})$ account for the spontaneous photons produced along transitions $|3\rangle \leftrightarrow |1\rangle$, and $|4\rangle \leftrightarrow |2\rangle$, respectively. The action of a Linblad operator is defined as: $L(C) = C\rho C^\dagger - \frac{1}{2}(\rho C^\dagger C + C^\dagger C\rho)$.

The terms proportional to Γ_{21}, and Γ_{12} arise from an incoherent relaxation process which couples states $|1\rangle \leftrightarrow |2\rangle$ bidirectionally. They arise from exchange interaction with the Fermi sea of holes in the back contact giving rise to spin-flip cotunneling. Let V_A and V_B be the gate voltages which determine the single hole charging region. For $V < V_A$ no hole is charged in the QD, whereas for $V > V_B$ the QD accommodates two holes. The state with the lowest energy depends on the gate voltage and the QD attempts to reach it by either attracting or repelling holes from or into the reservoir. The cotunneling at a certain gate voltage V_g in the absence of an external magnetic field can be shown to be given by[32]

$$\Gamma_{12} = \hbar\Gamma_t^2 \int_\epsilon \left| \frac{1}{\epsilon + q_e(V_g - V_A)/\lambda + i\frac{\hbar\Gamma_t}{2}} + \frac{1}{-\epsilon + q_e(V_g - V_A)/\lambda + i\frac{\hbar\Gamma_t}{2}} \right|^2 g(\epsilon)d\epsilon, \tag{6}$$

q_e, Γ_t and λ being the charge of the electron, the tunneling rate and a constant describing the geometric lever arm of the heterostructure, respectively. $g(\epsilon) = f(\epsilon)\left[1 - f(\epsilon)\right]$, $f(\epsilon)$ stands for the Fermi function: $f(\epsilon) = 1/\left[1 + exp(\epsilon/k_BT)\right]$, $k_B(T)$ being the Boltzman constant(temperature). ϵ stands for the detuning from the reservoir's Fermi energy ϵ_F of the hole state in the reservoir which couples with the hole in the QD to form a virtual state which finally relaxes producing the hole spin flip. The imaginary part in the denominator in Eq. (6) introduces a finite lifetime to the hole states given by Γ_t which is relevant for those regions of the integral with vanishing real part. Decay rate for relaxing from an energetically higher into a lower state is different from the opposite direction. The two processes are related by

thermal equilibrium and read as $\Gamma_{21} = \Gamma_{12} e^{-E^h_{Zm}/k_B T}$. The terms proportional to Γ_{43}, and Γ_{34} arise from a similar cotunneling process involving the trion states, and the following condition $\Gamma_{43} = \Gamma_{34} e^{-E^e_{Zm}/k_B T}$ holds.

The Hamiltonian in an appropriate rotating frame reads as

$$H = \hbar(\delta_3 - \delta_4 + \omega_{43})\sigma_{22} + \hbar\delta_3\sigma_{33} + \hbar(\delta_3 + \omega_{43})\sigma_{44} + \hbar\left(\Omega_3\sigma_{13} + \Omega_4\sigma_{24} + \Omega_N\sigma_{34} + H.c.\right) , \tag{7}$$

where $\delta_3 = \omega_{31} - \omega_{3L}$, and $\delta_4 = \omega_{42} - \omega_{4L}$ stand for the optical detunings. The equations of motion of the density matrix elements are derived in Appendix A.

Quantum optical experiments allow also to investigate the statistics of emitted light. Here we focus on the spectral properties of the fluorescent photons, in particular the so-called Resonance Fluorescence Spectrum (RFS) of the QDs. In the steady-state regime, this spectrum is proportional to the Fourier transformation of the correlation function $\lim_{t\to\infty}\langle E^-(r, t' + t) \cdot E^+(r, t)\rangle$, where $E^-(r, t)/E^+(r, t)$ is the negative/positive frequency part of the radiation field in the far zone. The radiation field consists of a free-field operator and a source-field operator that is proportional to the atomic polarization operator[34]. Therefore, the steady-state RFS can be expressed in terms of the atomic correlation function

$$S(\omega) = \Re\left[\lim_{t\to\infty}\int_0^\infty \langle E^+(t' + t) \cdot E^-(t)\rangle e^{-i\omega t'} dt'\right] , \tag{8}$$

where $\Re[\,]$ denotes the real part of the magnitude enclosed in square brackets, and $E^+(t)$ is the positive frequency part of the fluorescent field which in the far-field zone ($|\vec{r}| \gg c/\omega_{ij}$, $i = 4, 3$, $j = 1, 2$) reads

$$\vec{E}^+(\vec{r}, t) = \frac{\omega^2_{31}}{c^2|\vec{r}|}\vec{\mu}_{13}\sigma_{31}(t - |\vec{r}|/c) + \frac{\omega^2_{42}}{c^2|\vec{r}|}\vec{\mu}_{24}\sigma_{42}(t - |\vec{r}|/c) , \tag{9}$$

and $E^-(t) = (E^+(t))^\dagger$. We will assume that $\omega_{31} \approx \omega_{42}$. We remind here that the following conditions hold: $\vec{\mu}_{13} = \mu(\frac{\hat{u}_x}{\sqrt{2}} - i\frac{\hat{u}_y}{\sqrt{2}})$, $\vec{\mu}_{24} = \mu(\frac{\hat{u}_x}{\sqrt{2}} + i\frac{\hat{u}_y}{\sqrt{2}})$, whereas the direction of detection of the fluorescent field is perpendicular to the plane XY which contains the atomic dipole moments $\vec{\mu}_{13}$ and $\vec{\mu}_{24}$.

In writing Eq. (8), we abbreviate $\omega - \omega_{3L}(\omega - \omega_{4L})$ by ω, but we should interpret ω as a frequency measured relative to the laser frequency $\omega_{3L}(\omega_{4L})$ since we will assume that the QD is singly driven by $\Omega_3(\Omega_4)$. The calculation of $S(\omega)$ requires to evaluate two-time correlation

functions, which can be performed by means of the quantum-regression theorem[34,35] (see Appendix A for details). The RFS given in Eq. (8) has two contributions: one of them is due to the dipole operator σ_{31} (the term involving $\hat{U}_{13}(\tau)$ as defined in Appendix A), while the other arises from the dipole operator σ_{42} (the term involving $\hat{U}_{24}(\tau)$). The numerical solution of the equations of interest make use of a collection of scripts written in Octave[36].

III. NUMERICAL RESULTS

Let us start considering how the gate voltage V_g influences the cotunneling rates Γ_{12} and Γ_{34}. Previous studies on neutral excitons in n-doped QDs have shown that cotunneling rates are characterized by their nonlinear voltage dependence, showing an ultra-steep slope at the edges of the voltage plateau, and a weak dependence on voltage in the plateau center[37]. The results for negatively charged excitons also shown a similar trend[32]. Here we address the problem for the case of p-doped QDs in the absence of an external magnetic field. The decay rates obtained through Eq. (6) (not shown) reproduce quite well the results for the hole spin lifetime and the trion spin lifetime at the plateau center reported in Refs. 8 and 9 for the following set of parameters: $\Gamma_t = 0.433$ ns^{-1} for the hole states, $\Gamma_t = 0.137$ ns^{-1} for the trion states, and $V_A = -V_B = -50$ mV, $k_BT = 362\,\mu$eV, and $\lambda = 5$. Changing the gating voltage should result in the modification of the cotunneling rates by more than six orders of magnitude. We will show that the tuning of V should influence the linewidth of the Raman photons.

In order to study the Raman photons, we assume free space radiative decay rates of the transitions of $\hbar\Gamma_0 = 4.83\,\mu$eV. The magnitude $\hbar\Omega_N$ is taken to be $0.73\,\mu$eV which corresponds to an average internal Overhauser magnetic field of 21 mT. These data are obtained from experimental studies[8,9]. In what follows we also consider a single driving field Ω_3 non resonant with transition $|1\rangle \leftrightarrow |3\rangle$, i.e., $\delta_3 \neq 0$ and $\Omega_4 = 0$. Numerical results are displayed in Fig. 2(a) for $\Omega_3 = 1.5\Gamma_0$, and $\delta_3 = -5\Gamma_0$. We set the gate voltage to $V = -40$ mV, which is far from the plateau center, thus preventing hole spin pumping. Solid line corresponds to the contribution to RFS from the correlation $U_{13}(\tau)$ and exhibits a Mollow-like triplet. Most interestingly, dashed line represents the contribution to RFS from the correlation $U_{24}(\tau)$ and exhibit a two-peak structure: one of the peaks, the blue detuned which is close to $\omega = 0$, exhibit subnatural linewidth (the Raman photons) whereas the other peak has a linewidth

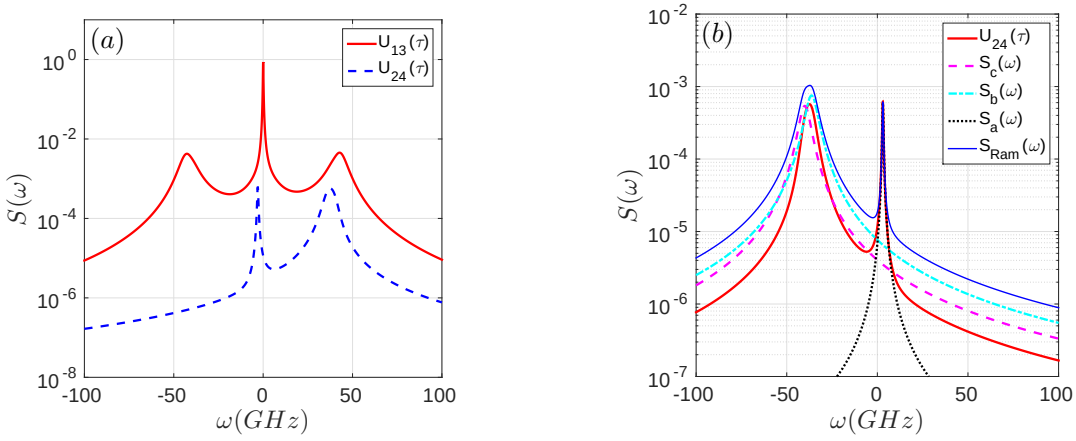

FIG. 2. Steady-state RFS ($S(\omega)$) versus ω of the out of resonance singly driven QD (Ω_3). (a) $\delta_3 = -5\Gamma_0$, $\Omega_3 = 1.5\Gamma_0$. Solid line(dashed line) represents the resonance fluorescence arising from correlation $U_{13}(\tau)$ ($U_{24}(\tau)$). The gating voltage was set to $V = -40$ mV. (b) RFS ($S(\omega)$) versus ω arising from correlation $U_{24}(\tau)$ (thick solid line) when $\delta_3 = +5\Gamma_0$, $\Omega_3 = 1.5\Gamma_0$. Lorentzians obtained in the dressed state basis (Eq. (B11)). Thin solid line is the RFS obtained as the sum of the three Lorentzians (Eq. (B10)).

close to Γ_0. The photons arising from these two correlations can be isolated by making use of a polarization selective detection geometry. Based on the characteristic of the current QD we estimated the FWHM of this peak to be in the order of 0.66 GHz, which is around eleven times lower than the value of the spontaneous emission rate ($\Gamma_0 = 7.33$ GHz). Most interestingly, the narrow spectral feature can be tuned by changing the detuning of the external laser as shown in Fig. 2(b) which demonstrates the appearance of a red detuned subnatural peak for the Raman photons (thick solid line) when the detuning of the driving laser is set to $\delta_3 = +5\Gamma_0$ while keeping fixed the rest of parameters. It is worth noting that the Overhauser field is responsible for the appearance of such narrow spectral feature: in the case of setting $\Omega_N = 0$ (which is a meaningless physical situation), the spontaneous photons (Raman photons) cannot decay to level $|2\rangle$ since levels $|3\rangle$ and $|4\rangle$ eventually decouple one another.

The RFS in the Dressed State Picture (DSP) for the Raman photons is obtained in Appendix B when $\delta_3 \neq 0$. There it is shown that RFS of the Raman photons arises from correlation $U_{24}(\tau)$, and we show that in the secular approximation the RFS for the photons produced along $|2\rangle \leftrightarrow |4\rangle$ channel can be described as transitions between states of adjacent

manifolds: from state $|j, N\rangle$ to $|2, N-1\rangle$, $j = a', b', c'$, N being the number of photons. Equation (B10) shows that RFS is given as a sum of three different Lorentzians. In the case of $\delta_3 < 0$, the Raman photons line is obtained through the transition $|c'\rangle \leftrightarrow |2\rangle$: it is centered at $\omega = -\lambda_3$, and the linewidth is $2\Gamma_{c'2}$. In the case with $\delta_3 > 0$ the Raman photons line arise from transition $|a'\rangle \leftrightarrow |2\rangle$, is centered at $\omega = -\lambda_1$ and the linewidth is $2\Gamma_{a'2}$. The amplitudes of the different Lorentzians are obtained by solving Eqs. (B3)-(B5). Figure 2(b) also show the individual Lorentzians obtained for that particular situation, demonstrating the adequacy of the description in the DSP which catch the peaks positions and reproduces the shape of the spectrum. We checked that the FWHM of $S_a(\omega)$ is $2\Gamma_{a'2} = 0.656$ GHz, in good agreement with the numerical determination using the full RFS.

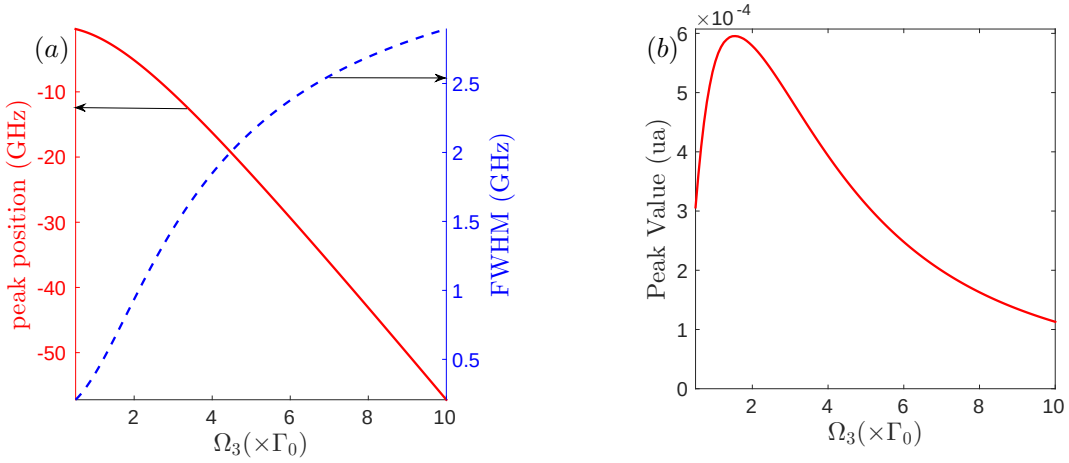

FIG. 3. (a) Peak position of the Raman photons ($-\lambda_3$) in GHz measured relative to ω_{3L} versus the Rabi frequency of the driving field Ω_3 (solid line), and FWHM of the Raman photon line ($2\Gamma_{c'2}$) versus Rabi frequency of the driving field Ω_3 (dashed line) for $\delta_3 = -5\Gamma_0$. (b) Peak value of the Raman photon line ($max(S_c(\omega))$) versus Rabi frequency of the driving field Ω_3 for $\delta_3 = -5\Gamma_0$.

The Rabi frequency of the driving field Ω_3 can be also used as a knob to tune the peak location and linewidth of the Raman photons line. Such tunability is shown with solid line in Fig. 3(a) which was produced while keeping constant $\delta_3 = -5\Gamma_0$, and $V = -40$ mV. In addition, we also plot in the same panel the FWHM in GHz of this spectral feature. These curves where obtained through the values of λ_3 and $\Gamma_{c'2}$, respectively, as defined in Appendix B. This figure reveals that large changes of the peak location are obtained at the expense of increasing the linewidth, which however remains subnatural. This increase of the linewidth is just a consequence of power broadening. The negative value for the peak

position is just an indication that the Raman photons are blue detuned with regard to the laser field. Figure 3(b) shows the peak value, i.e., the maximum value of $S_c(\omega)$, in arbitrary units versus the Rabi frequency of the driving field. This curve shows the existence of a Rabi frequency which maximizes the signal of the Raman line. The use of a large value for $\delta_3 = -10\Gamma_0$ also allows to obtain a large degree of tunability, in the order of 44 GHz for the largest Rabi frequency accompanied by a slight reduction of the maximum linewidth up to 2.2 GHz. In this case the maximum signal shifts to large values of Ω_3. In summary, the Raman photons signal can be tuned by changing the detuning and/or the Rabi frequency of the driving field.

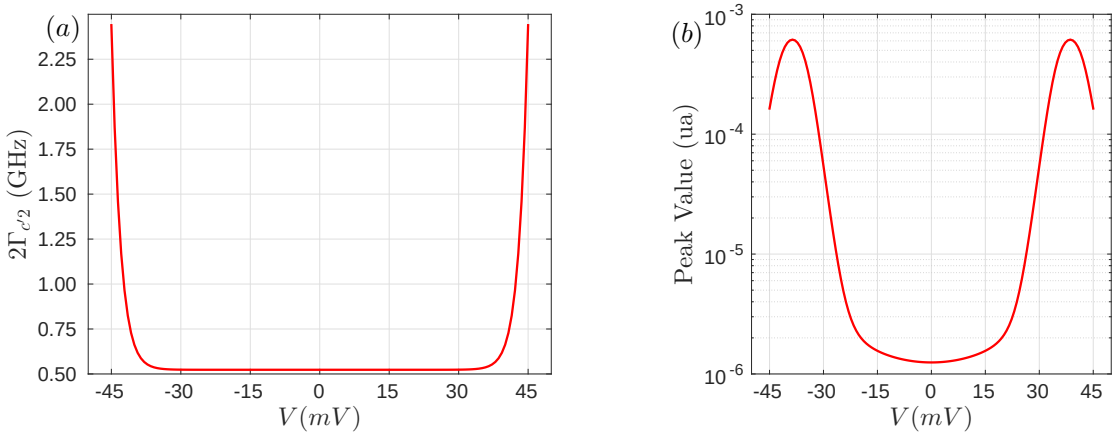

FIG. 4. (a) FWHM of the Raman photon line ($2\Gamma_{c'2}$) versus the gate voltage. (b) Peak value Peak value of the Raman photon line ($max(S_c(\omega))$) versus the gate voltage. $\Omega_3 = 1.5\Gamma_0$, and $\delta_3 = -5\Gamma_0$.

A change of the gating voltage results in the modification of the cotunneling of the lower and upper levels. This in turn results in changes in the linewidth and the peak value of the Raman line as depicted in Fig. 4. These curves where produced while keeping constant the Rabi frequency and the detuning of the driving field. Here we observe a non-linear character of the linewidth when the gate voltage is changed, while it remains almost constant at the voltage plateau. This result can be explained by the nonlinearity of the cotunneling rates given by Eq. (6). The reduction in the linewidth at the center of the voltage plateau (where efficient optical pumping is obtained) is accompanied by a drop of the peak value of the Raman line by more than two orders of magnitude.

One may wonder whether spectral fluctuations (SD)[38] should affect the spontaneous Raman photons. Signatures of of such influence on the RFS in QDs have been experimentally

found[39–41]. In what follows we assume that the effect of SD can be accounted for by considering a Gaussian weighting function $W(\delta_3) = exp\left[-1/2\,(\delta_3/\Delta_{diff})^2\,8\ln 2\right]$, Δ_{diff} being the diffusion coefficient, thus the effective RFS is obtained as a convolution of the unweighted RFS (obtained from Eq. (A6)) and the Gaussian line shape $W(\delta_3)$. Matthiesen et al. 39 have provided experimental evidence that Δ_{diff} depends on the average excitation detuning (δ_3 in our notation). Assuming a value of $\Delta_{diff} \approx 140$ MHz, we computed the linewidth of the resulting Raman photon line which after convolution shows very minor changes in the width (in the second decimal place) in relation to the unweighted spectrum. This results is expected: when convolving two functions of very different width, the one with the largest width ($2\Gamma_{c'2}$) dominates over the other (Δ_{diff}).

IV. CONCLUSIONS

In this work we present a theoretical description of the spontaneous Raman photons in singly charged p-doped QDs. The QDs are modeled as a four level-like atomic system where the interaction of the electron spin with the nuclei of the QD is taken into account using a frozen model for the nuclear spins. We present numerical simulations using data taken from experimental studies which show that the center and linewidth of the Raman photon line can be changed by all optical methods by changing either the detuning and/or the Rabi frequency of the far detuned driving laser. We also analyze the influence of the gating voltage on the linewidth and the peak value of the fluorescent signal. In contrast with n-doped quantum dots, the current scheme does not require the application of an external magnetic field, making the current system a candidate for quantum information applications.

Appendix A: Appendix A: Density matrix equations of motion and RFS in the bare state basis

The equations of motion of the density matrix elements are obtained through $\dot{\rho} = -\frac{i}{h}[H,\rho] + \mathcal{L}\rho$, and are rewritten in terms of time averaged σ operators for convenience, and read

$$
\begin{aligned}
\frac{\partial\langle\sigma_{22}\rangle}{\partial t} &= (\Gamma_0-\Gamma_{12})\langle\sigma_{44}\rangle-(\Gamma_{12}+\Gamma_{21})\langle\sigma_{22}\rangle-\Gamma_{12}\langle\sigma_{33}\rangle+\Gamma_{12}\\
&\quad -i\Omega_4\langle\sigma_{24}\rangle+i\Omega_4^*\langle\sigma_{42}\rangle\,,\\
\frac{\partial\langle\sigma_{33}\rangle}{\partial t} &= -(\Gamma_{34}+\Gamma_0)\langle\sigma_{33}\rangle+\Gamma_{43}\langle\sigma_{44}\rangle\\
&\quad +i\Omega_3\langle\sigma_{13}\rangle-i\Omega_3^*\langle\sigma_{31}\rangle-i\Omega_N\langle\sigma_{34}\rangle+i\Omega_N\langle\sigma_{43}\rangle\,,\\
\frac{\partial\langle\sigma_{44}\rangle}{\partial t} &= \Gamma_{34}\langle\sigma_{33}\rangle-(\Gamma_{43}+\Gamma_0)\langle\sigma_{44}\rangle\\
&\quad +i\Omega_4\langle\sigma_{24}\rangle-i\Omega_4^*\langle\sigma_{42}\rangle+i\Omega_N\langle\sigma_{34}\rangle-i\Omega_N\langle\sigma_{43}\rangle\,,\\
\frac{\partial\langle\sigma_{12}\rangle}{\partial t} &= -F_{12}\langle\sigma_{12}\rangle+i\Omega_3^*\langle\sigma_{32}\rangle-i\Omega_4\langle\sigma_{14}\rangle\,,\\
\frac{\partial\langle\sigma_{13}\rangle}{\partial t} &= -F_{13}\langle\sigma_{13}\rangle+i\Omega_3^*(\langle\sigma_{33}\rangle-\langle\sigma_{11}\rangle)-i\Omega_N\langle\sigma_{14}\rangle\,,\\
\frac{\partial\langle\sigma_{14}\rangle}{\partial t} &= -F_{14}\langle\sigma_{14}\rangle-i\Omega_4^*\langle\sigma_{12}\rangle+i\Omega_3^*\langle\sigma_{34}\rangle-i\Omega_N\langle\sigma_{13}\rangle\,,\\
\frac{\partial\langle\sigma_{23}\rangle}{\partial t} &= -F_{23}\langle\sigma_{23}\rangle-i\Omega_3^*\langle\sigma_{21}\rangle+i\Omega_4^*\langle\sigma_{43}\rangle-i\Omega_N\langle\sigma_{24}\rangle\,,\\
\frac{\partial\langle\sigma_{24}\rangle}{\partial t} &= -F_{24}\langle\sigma_{24}\rangle+i\Omega_4^*(\langle\sigma_{44}\rangle-\langle\sigma_{22}\rangle)-i\Omega_N\langle\sigma_{23}\rangle\,,\\
\frac{\partial\langle\sigma_{34}\rangle}{\partial t} &= -F_{34}\langle\sigma_{34}\rangle+i\Omega_3\langle\sigma_{14}\rangle-i\Omega_4^*\langle\sigma_{32}\rangle+i\Omega_N(\langle\sigma_{44}\rangle-\langle\sigma_{33}\rangle)\,.
\end{aligned}
\tag{A1}
$$

To obtain the above equations we made use of the following definition for the generalized dephasings: $F_{12}=(\Gamma_{12}+\Gamma_{21})/2+i(\delta_3-\delta_4-E^e_{Zm})$, $F_{13}=(\Gamma_{12}+\Gamma_{34}+\Gamma_0)/2+i\delta_3$, $F_{14}=(\Gamma_{12}+\Gamma_{43}+\Gamma_0)/2+i(\delta_3-E^e_{Zm})$, $F_{23}=(\Gamma_{21}+\Gamma_{34}+\Gamma_0)/2+i(\delta_4+E^e_{Zm})$, $F_{24}=(\Gamma_{21}+\Gamma_{43}+\Gamma_0)/2+i\delta_4$, $F_{34}=(\Gamma_{43}+\Gamma_{34}+2\Gamma_0)/2-iE^e_{Zm}$. We also assume that we are dealing with a closed system, i.e., $\langle\sigma_{11}\rangle+\langle\sigma_{22}\rangle+\langle\sigma_{33}\rangle+\langle\sigma_{44}\rangle=1$. In writing Eq. (A1) we take into account that $\rho_{kl}(t)=\langle\sigma_{lk}(t)\rangle$.

Let us define the vector $U(t)=[\sigma_{22}(t),\,\sigma_{33}(t),\,\sigma_{44}(t),\,\sigma_{12}(t),\,\sigma_{21}(t),\,\sigma_{13}(t),\,\sigma_{31}(t),\,\sigma_{14}(t),\,\sigma_{41}(t),\,\sigma_{23}(t),\,\sigma_{32}(t),\,\sigma_{24}(t),\,\sigma_{42}(t),\,\sigma_{34}(t),\,\sigma_{43}(t)]^T$, where T stands for transpose. Thus Eq. (A1) can be written in matrix form as

$$
\frac{d\,U(t)}{d\,t}=MU(t)+B\,,
\tag{A2}
$$

M being a 15×15 matrix of coefficients and B the independent term which can be easily derived from Eq. (A1).

The evaluation of the two-time correlation functions that appear in Eq. (8) can be recast

to

$$S(\omega) = f^2(r)|\mu|^2 \Re \left[\int_0^\infty \left(\langle \sigma_{31}(\tau)\sigma_{13}(\infty)\rangle + \langle \sigma_{42}(\tau)\sigma_{24}(\infty)\rangle \right) e^{-i\omega\tau} d\tau \quad \right] . \tag{A3}$$

The two-time correlation functions which appear in Eq. (A3) can be determined with the aid of the quantum regression theorem[34,35] and the optical Bloch Eq. (A1). To this end we define the column vector

$$\begin{aligned} \hat{U}_{jk}(\tau) = [&\langle \sigma_{22}(\tau)\sigma_{jk}(\infty)\rangle, \ \langle \sigma_{33}(\tau)\sigma_{jk}(\infty)\rangle, \\ &\langle \sigma_{44}(\tau)\sigma_{jk}(\infty)\rangle, \langle \sigma_{12}(\tau)\sigma_{jk}(\infty)\rangle, \\ &\langle \sigma_{21}(\tau)\sigma_{jk}(\infty)\rangle, \langle \sigma_{13}(\tau)\sigma_{jk}(\infty)\rangle, \\ &\langle \sigma_{31}(\tau)\sigma_{jk}(\infty)\rangle, \langle \sigma_{14}(\tau)\sigma_{jk}(\infty)\rangle, \\ &\langle \sigma_{41}(\tau)\sigma_{jk}(\infty)\rangle, \langle \sigma_{23}(\tau)\sigma_{jk}(\infty)\rangle, \\ &\langle \sigma_{32}(\tau)\sigma_{jk}(\infty)\rangle, \langle \sigma_{24}(\tau)\sigma_{jk}(\infty)\rangle, \\ &\langle \sigma_{42}(\tau)\sigma_{jk}(\infty)\rangle, \langle \sigma_{34}(\tau)\sigma_{jk}(\infty)\rangle, \\ &\langle \sigma_{43}(\tau)\sigma_{jk}(\infty)\rangle]^T \ , (j=1,k=3) \, , (j=2,k=4) \, . \end{aligned} \tag{A4}$$

where the super-index T stands for transpose. According to the quantum regression theorem, for $\tau > 0$ the vector $\hat{U}_{jk}$ satisfies

$$\frac{d\,\hat{U}_{jk}(\tau)}{d\tau} = M\hat{U}_{jk}(\tau) + B\langle \sigma_{jk}(\infty)\rangle \, . \tag{A5}$$

By working in the Laplace space we obtain the steady-state resonance fluorescence spectrum. Specifically we have

$$\begin{aligned} S(\omega) \propto \Gamma_0 \Re \Bigg\{ &\sum_{l=1}^{l=15} R_{7,l}(iz) \left(\hat{U}_{13}^{(l)}(\infty) + B\frac{\langle \sigma_{jk}(\infty)\rangle}{iz} \right) \\ &+ \sum_{l=1}^{l=15} R_{13,l}(iz) \left(\hat{U}_{24}^{(l)}(\infty) + B\frac{\langle \sigma_{jk}(\infty)\rangle}{iz} \right) \Bigg\} \ , \end{aligned} \tag{A6}$$

where $\hat{U}_{jk}^{(l)}(\infty)$ is the value of the $l-$th component of the vector $\hat{U}_{jk}(\tau)$ evaluated at $\tau = 0$, i.e., in the steady-state. $R_{jk}(iz)$ is the (j,k) element of the matrix $R(iz)$ defined as

$$R(iz) = \left(iz\hat{I} - M \right)^{-1} , \tag{A7}$$

$\hat{I}$ being the 15×15 identity matrix, and $z \equiv (\omega - \omega_{3L})/\Gamma_0$.

Appendix B: Appendix B: Raman photons in the dressed state basis

Here we address the problem of computing the RFS in the dressed state picture for the case of using a single driving field ($\Omega_3 \neq 0$, and $\Omega_4 = 0$) when the system is driven out of resonance ($\delta_3 \neq 0$) and with no external magnetic field, i.e., $B = 0$. This simple case allows for the obtention of an analytical expression for the spectrum of the emitted Raman photons. The atomic and coherent part of the Hamiltonian reads

$$H = \hbar\delta_3\sigma_{33} + \hbar\delta_3\sigma_{44} + \hbar\left(\Omega_3\sigma_{13} + \Omega_N\sigma_{34} + H.c.\right) . \tag{B1}$$

The eigenvalues are obtained through the roots of the following polynomial: $-\lambda^3 + 2\delta_3\lambda^2 - \lambda(\delta_3^2 - \Omega_N^2 - \Omega_3^2) - \Omega_3^2\delta_3$, and are labeled as $\lambda_j\,(j = 1, 2, 3)$. They are sorted in ascending order, i.e., $|\lambda_3| < |\lambda_2| < |\lambda_1|$. The corresponding eigenstates are

$$\begin{aligned} |a'\rangle &= a_1|1\rangle + a_3|3\rangle + a_4|4\rangle\,, \\ |b'\rangle &= b_1|1\rangle + b_3|3\rangle + b_4|4\rangle\,, \\ |c'\rangle &= c_1|1\rangle + c_3|3\rangle + c_4|4\rangle\,, \\ |d'\rangle &= |2\rangle\,. \end{aligned} \tag{B2}$$

The coefficients are given by $a_1 = \frac{\Omega_3}{A_1\lambda_1}$, $a_3 = \frac{1}{A_1}$, and $a_4 = -\frac{\Omega_N}{A_1(\delta_3-\lambda_1)}$, where $A_1 = \sqrt{1 + (\Omega_3/\lambda_1)^2 + (\Omega_N/(\delta_3 - \lambda_1))^2}$. The coefficients $b_j(c_j)$ are obtained from a_j by making the replacement $\lambda_1 \to \lambda_2(\lambda_3)$.

The emitted Raman photons are related with the correlation function $U_{24}(\tau) = \langle\sigma_{42}(\tau)\sigma_{24}(\infty)\rangle$. In the secular approximation this correlation reduces to $U_{24}(\tau) \approx a_4^2\langle\sigma_{a'2}(\tau)\sigma_{2a'}(\infty)\rangle + b_4^2\langle\sigma_{b'2}(\tau)\sigma_{2b'}(\infty)\rangle + c_4^2\langle\sigma_{c'2}(\tau)\sigma_{2c'}(\infty)\rangle$, and can be computed using the quantum regression theorem. Thus, we need the equations of motion of population and coherences of the dressed states in Eq. (B2) which are derived in the secular approximation. The equations of interest

read

$$\frac{d\langle\sigma_{a'a'}(t)\rangle}{dt} = \Gamma_{a'a'}\langle\sigma_{a'a'}\rangle + \Gamma_{a'b'}\langle\sigma_{b'b'}\rangle + \Gamma_{a'c'}\langle\sigma_{c'c'}\rangle + \Gamma^0_{a'a'}\,, \tag{B3}$$

$$\frac{d\langle\sigma_{b'b'}(t)\rangle}{dt} = \Gamma_{b'a'}\langle\sigma_{a'a'}\rangle + \Gamma_{b'b'}\langle\sigma_{b'b'}\rangle + \Gamma_{b'c'}\langle\sigma_{c'c'}\rangle + \Gamma^0_{b'b'}\,, \tag{B4}$$

$$\frac{d\langle\sigma_{c'c'}(t)\rangle}{dt} = \Gamma_{c'a'}\langle\sigma_{a'a'}\rangle + \Gamma_{c'b'}\langle\sigma_{b'b'}\rangle + \Gamma_{c'c'}\langle\sigma_{c'c'}\rangle + \Gamma^0_{c'c'}\,, \tag{B5}$$

$$\frac{d\langle\sigma_{a'2}(t)\rangle}{dt} = -\Gamma_{a'2}\langle\sigma_{a'2}\rangle\,, \tag{B6}$$

$$\frac{d\langle\sigma_{b'2}(t)\rangle}{dt} = -\Gamma_{b'2}\langle\sigma_{b'2}\rangle\,, \tag{B7}$$

$$\frac{d\langle\sigma_{c'2}(t)\rangle}{dt} = -\Gamma_{c'2}\langle\sigma_{c'2}\rangle\,, \tag{B8}$$

with

$$\begin{aligned}
\Gamma_{a'a'} &= -(\Gamma_{12}+\Gamma_{21})a_1^2 + (\Gamma_{34}+\Gamma_{43})a_3^2a_4^2 + \Gamma_0 a_1^2a_3^2 - (\Gamma_{34}+\Gamma_0)a_3^2 - (\Gamma_{43}+\Gamma_0)a_4^2\,,\\
\Gamma_{a'b'} &= -\Gamma_{21}a_1^2 + \Gamma_{34}a_4^2b_3^2 + \Gamma_{43}a_3^2b_4^2 + \Gamma_0 a_1^2b_3^2\,,\\
\Gamma_{a'c'} &= -\Gamma_{21}a_1^2 + \Gamma_{34}a_4^2c_3^2 + \Gamma_{43}a_3^2c_4^2 + \Gamma_0 a_1^2c_3^2\,,\\
\Gamma^0_{a'a'} &= \Gamma_{21}a_1^2\,,\\
\Gamma_{b'a'} &= -\Gamma_{21}b_1^2 + \Gamma_{34}b_4^2a_3^2 + \Gamma_{43}b_3^2a_4^2 + \Gamma_0 b_1^2a_3^2\,,\\
\Gamma_{b'b'} &= -(\Gamma_{12}+\Gamma_{21})b_1^2 + (\Gamma_{34}+\Gamma_{43})b_3^2b_4^2 + \Gamma_0 b_1^2b_3^2 - (\Gamma_{34}+\Gamma_0)b_3^2 - (\Gamma_{43}+\Gamma_0)b_4^2\,,\\
\Gamma_{b'c'} &= -\Gamma_{21}b_1^2 + \Gamma_{34}b_4^2c_3^2 + \Gamma_{43}b_3^2c_4^2 + \Gamma_0 b_1^2c_3^2\,,\\
\Gamma^0_{b'b'} &= \Gamma_{21}b_1^2\,,\\
\Gamma_{c'a'} &= -\Gamma_{21}c_1^2 + \Gamma_{34}c_4^2a_3^2 + \Gamma_{43}c_3^2a_4^2 + \Gamma_0 c_1^2a_3^2\,,\\
\Gamma_{c'b'} &= -\Gamma_{21}c_1^2 + \Gamma_{34}c_4^2b_3^2 + \Gamma_{43}c_3^2b_4^2 + \Gamma_0 c_1^2b_3^2\,,\\
\Gamma_{c'c'} &= -(\Gamma_{12}+\Gamma_{21})c_1^2 + (\Gamma_{34}+\Gamma_{43})c_3^2c_4^2 + \Gamma_0 c_1^2c_3^2 - (\Gamma_{34}+\Gamma_0)c_3^2 - (\Gamma_{43}+\Gamma_0)c_4^2\,,\\
\Gamma^0_{c'c'} &= \Gamma_{21}c_1^2\,,\\
\Gamma_{a'2} &= \Gamma_{21}/2 + \Gamma_{12}a_1^2/2 + (\Gamma_{34}+\Gamma_0)a_3^2/2 + (\Gamma_{43}+\Gamma_0)a_4^2/2\,,\\
\Gamma_{b'2} &= \Gamma_{21}/2 + \Gamma_{12}b_1^2/2 + (\Gamma_{34}+\Gamma_0)b_3^2/2 + (\Gamma_{43}+\Gamma_0)b_4^2/2\,,\\
\Gamma_{c'2} &= \Gamma_{21}/2 + \Gamma_{12}c_1^2/2 + (\Gamma_{34}+\Gamma_0)c_3^2/2 + (\Gamma_{43}+\Gamma_0)c_4^2/2\,.
\end{aligned} \tag{B9}$$

The spectrum of the Raman photons are finally derived making use of the Laplace transform for the correlation function $U_{24}(\tau)$, and reads

$$S_{Ram}(\omega) = S_a(\omega) + S_b(\omega) + S_c(\omega)\,, \tag{B10}$$

where

$$
\begin{aligned}
S_a(\omega) &= \Re\left\{ a_4^2 \frac{\langle \sigma_{a'a'}(\infty)\rangle}{\Gamma_{a'2} - i(\omega+\lambda_1)} \right\}, \\
S_b(\omega) &= \Re\left\{ b_4^2 \frac{\langle \sigma_{b'b'}(\infty)\rangle}{\Gamma_{b'2} - i(\omega+\lambda_2)} \right\}, \\
S_c(\omega) &= \Re\left\{ c_4^2 \frac{\langle \sigma_{c'c'}(\infty)\rangle}{\Gamma_{c'2} - i(\omega+\lambda_3)} \right\}.
\end{aligned}
\tag{B11}
$$

ACKNOWLEDGMENTS

This work has been supported by Project no. FIS2013-41709-P (MICINN) from Spain. The authors thank Complutense University for financial support with grant reference GR3/14-910133.

The authors are specially indebted to Tomás Lorca for revising the manuscript.

---

[1] D. Loss, and D. P. DiVincenzo, Phys. Rev. A 57, 120 (1998).

[2] N. H. Bonadeo, J. Erland, D. Gammon, D. Park, D. S. Parker, D. G. Steel, Science 282, 1473 (1998).

[3] M. Atatüre J. Dreiser, A. Badolato, A. Högele, K. Karrai, A. Imamoglu, Science 312, 551 (2006).

[4] X. Xu, Y. Wu, B. Sun, Q. Huang, J. Cheng, D. G. Steel, A. S. Bracker, D. Gammon, C. Emary, L. J. Sham, Phys. Rev. Lett. 99, 097401 (2007).

[5] C. Emary, X. Xu, D. G. Steel, S. Saikin, L. J. Sham, Phys. Rev. Lett. 98, 047401 (2007).

[6] V. Loo, L. Lanco, O. Krebs, P. Senellart, P. Voisin, Phys. Rev. B 83, 033301 (2011).

[7] B. D. Gerardot, D. Brunner, P. A. Dalgarno, P. Öhberg, S. Seidl, M. Kroner, K. Karrai, N. G. Stoltz, P. M. Petroff, R. J. Warburton, Nature 451, 441 (2008).

[8] D. Brunner, B. D. Gerardot, P. A. Dalgarno, G. Wüst, K. Karrai, N. G. Stoltz, P. M. Petroff, R. J. Warburton, Science 325, 70 (2009).

[9] D. Brunner, Ph.D. Thesis, Herior-Watt University, 2010, `http://hdl.handle.net/10399/2350`.

[10] Y. Wu, E. D. Kim, X. Xu, J. Cheng, D. G. Steel, A. S. Bracker, D. Gammon, S. E. Economou, L. J. Sham, Phys. Rev. Lett. 99, 097402 (2007).

[11] A. J. Ramsay, S. J. Boyle, R. S. Kolodka, J. B. B. Oliveira, J. Skiba-Szymanska, H. Y. Liu, M. Hopkinson, A. M. Fox, M. S. Skolnick, Phys. Rev. Lett. 100, 197401 (2008).

[12] D. Press, T. D. Ladd, B. Zhang, Y. Yamamoto, Nature 456, 218 (2008).

[13] K. Greve, P. L. McMahon, D. Press, T. D. Ladd, D. Bisping, C. Schneider, M. Kamp, L. Worschech, S. Höfling, A. Forchel, Y. Yamamoto, Nat. Phys. 7, 872 (2011).

[14] A. Muller, E. B. Flagg, P. Bianucci, X. Y. Wang, D. G. Deppe, W. Ma, J. Zhang, G. J. Salamo, M. Xiao, C. K. Shih, Phys. Rev. Lett. 99, 187402 (2007).

[15] A. N. Vamivakas, Y. Zhao, Chao-Yang Lu, M. Atatüre, Nat. Phys. 5, 198 (2009).

[16] E. B. Flagg, A. Muller, J. W. Robertson, S. Founta, D. G. Deppe, M. Xiao, W. Ma, G. J. Salamo, C. K. Shih, Nat. Phys. 5, 203 (2009).

[17] S. T. Yilmaz, P. Fallahi, A. Imamoglu, Phys. Rev. Lett. 105, 033601 (2010).

[18] P. Fallahi, S. T. Yilmaz, A. Imamoglu, Phys. Rev. Lett. 105, 257402 (2010).

[19] A. Ulhaq, S. Weiler, C. Roy, S. M. Ulrich, M. Jetter, S. Hugues, P. Michler, Opt. Express 21, 4382 (2013).

[20] R-C. Ge, S. Weiler, A. Ulhaq, S. M. Ulrich, M. Jetter, P. Michler, S. Hugues, Opt. Lett. 15, 1691 (2013).

[21] C.-Y. Lu, Y. Zhao, A. N. Vamivakas, C. Matthiesen, S. Fält, A. Badolato, M. Atatüre, Phys. Rev. B 81, 035332 (2010).

[22] H. S. Nguyen, G. Sallen, C. Voisin, Ph. Roussignol, C. Diederichs, G. Cassabois, Appl. Phys. Lett. 99, 261904 (2011).

[23] C. Matthiesen, A. N. Vamivakas, M. Atatüre, Phys. Rev. Lett. 108, 093602 (2012).

[24] K. Konthasinghe, M. Peiris, B. Petrak, Y. Yu, Z. C. Niu, A. Muller, Opt. Lett. 40, 1846 (2015).

[25] C. Cabrillo, J. I. Cirac, P. García-Fernández, P. Zoller, Phys. Rev. Lett. 59, 1025 (1999).

[26] D. L. Moehring, P. Maunz, S. Olmschenk, K. C. Younge, D. N. Matsukevich, L. -M. Duan, C. Monroe, Nature 449, 68 (2007).

[27] J. Hofmann, M. Krug, N.t Ortegel, L. Gérard, M. Weber, W. Rosenfeld, H. Weinfurter, Science 337, 72 (2012).

[28] H. Bernien, B. Hensen, W. Pfaff, G. Koolstra, M. S. Blok, L. Robledo, T. H. Taminiau, M. Markham, D. J. Twitchen, L. Childress, R. Hanson, Nature 497, 86 (2013).

[29] A. Delteil, Z. Sun, W-B. Gao, E. Togan, S. Faelt, A. Imamoglu, Nat. Phys. doi:10.1038/NPHYS3605.

[30] G. Fernandez, T. Volz, R. Desbuquois, A. Badolato, A. Imamoglu, Phys. Rev. Lett. 103, 087406 (2009).

[31] I. A. Merkulov, Al. L. Efros, M. Rosen, Phys. Rev. A 65, 205309 (2002).

[32] J. Dreiser, M. Atatüre, C. Galland, T. Müller, A. Badolato, A. Imamoglu, Phys. Rev. B 77, 075317 (2008).

[33] P. Maletinsky, A. Badolato, A. Imamoglu, Phys. Rev. Lett. 99, 056804 (2007).

[34] M. O. Scully, M. S. Zubairy, Quantum Optics, 1997 Cambridge University Press.

[35] M. Lax, Phys. Rev. 172, 350 (1968).

[36] J. W. Eaton, D. Bateman, S. Hauberg, R. Wehbring, GNU Octave version 3.8.1 manual: a high-level interactive language for numerical computations, 2014 CreateSpace Independent Publishing Platform.

[37] J. M. Smith, P. A. Dalgarno, R. J. Warburton, A. O. Govorov, K. Karrai, B. D. Gerardot, P. M. Petroff, Phys. Rev. Lett. 94, 197402 (2005).

[38] S. A. Empedocles, M. G. Bawendi, Science 278, 2114 (1997).

[39] C. Matthiesen, M. J. Stanley, M. Hugues, E. Clarke, M. Atatüre, Sci. Rep. 4, 1991 (2014).

[40] A. Majumdar, E. D. Kim, J. Vučković, Phys. Rev. B 84, 195304 (2011).

[41] K. Konthasinghe, J. Walker, M. Peiris, C. K. Shih, Y. Yu, M. F. Li, J. F. He, L. J. Wang, H. Q. Ni, Z. C. Niu, A. Muller Phys. Rev. B 85, 235315 (2012).